Coupled Geomechanical and Geochemical Responses of Carbonate-Bearing Sandstone Reservoirs to CO_2 Injection: A Critical Review of Instability Mechanisms, Risk-Assessment Frameworks, and Implications for Energy Storage

Raymond Aderoju[1]*, Moses Falowo[2], Olaniyi Anisere[3], Olasunkanmi Olagboye[4]

[1]Department of Geology, University of Georgia, Georgia, USA

[2]Department of Geology, Kansas State University, Kansas, USA

[3]Department of Geology and Geophysics, Louisiana State University, Louisiana, USA

[4]Department of Applied Geology, Federal University of Technology Akure, Nigeria

***Corresponding Author**

DOI: https://doi.org/10.51584/IJRIAS.2026.11070099

Received: 22 July 2026; Accepted: 27 July 2026; Published: 05 August 2026

ABSTRACT

The safe and permanent geological storage of carbon dioxide (CO_2) in deep carbonate-bearing sandstone formations requires a rigorous understanding of the coupled geomechanical and geochemical responses of the host reservoir to sustained fluid injection. Fluid injection simultaneously raises pore pressure, reduces effective stress on pre-existing faults, triggers carbonate mineral dissolution under acidic CO_2-saturated brine, and drives heterogeneous permeability evolution, a set of interdependent processes whose combined effect on reservoir integrity, cap-rock seal security, and induced seismicity risk is not adequately captured by existing single-process risk assessment frameworks. This comprehensive review synthesizes 96 peer-reviewed studies published between 1980 and 2024 to characterize the mechanistic basis and field-scale consequences of these coupled responses in carbonate-bearing sandstones. We examine: (i) the theoretical framework linking pore pressure increase, Biot effective stress reduction, and Coulomb failure on critically stressed faults; (ii) the geochemistry of carbonate dissolution under CO_2-acidified brine, including reaction kinetics, dissolution regimes, and their dependence on mineralogical composition; (iii) the coupled evolution of permeability anisotropy under combined mechanical and chemical loading; (iv) the mechanisms of cap-rock integrity failure including hydraulic fracturing, fault reactivation, capillary leakage, and wellbore cement degradation; (v) quantitative evidence from active geological carbon storage (GCS) sites including Sleipner, In Salah, Decatur, and Otway; and (vi) the limitations of current continuum-scale risk assessment practice. We identify four critical gaps in the literature and propose a six-phase integrated geomechanical-geochemical risk assessment framework for GCS operations in carbonate-bearing formations. The framework directly addresses the systematic underestimation of geomechanical instability risk arising from the failure to couple dissolution-driven permeability evolution with mechanical stability analysis in current engineering practice.

Keywords: Geological carbon storage, Carbonate dissolution, Fault reactivation and induced seismicity, Cap-rock integrity, Permeability evolution and effective stress

Table G1. Glossary of abbreviations and technical terms used throughout this review.

Term	Definition
GCS	Geological Carbon Storage

ISSN No. 2454-6194 | DOI: 10.51584/IJRIAS |Volume XI Issue VII July 2026

CFS / ΔCFS	Coulomb failure stress / change in Coulomb failure stress
MAP	Maximum allowable (injection) pressure
TLP	Traffic light protocol (seismicity-based injection management)
α (Biot–Willis coefficient)	Poroelastic coupling coefficient linking pore pressure to effective stress
Wormholing	Localized, channelized dissolution pathway that produces highly anisotropic permeability enhancement
Pe (capillary entry pressure)	Threshold pressure at which a non-wetting fluid (CO_2) can invade a water-wet, fine-pored cap-rock
Reactive surface area (As)	Mineral surface area actually exposed to and participating in dissolution reactions
Rate-and-state friction	Friction framework describing whether a stressed fault slips seismically or creeps aseismically

INTRODUCTION

Geological carbon storage (GCS) in deep saline aquifers and carbonate-bearing sandstone formations is a cornerstone technology in the portfolio of strategies required to meet the climate targets of the Paris Agreement. The Intergovernmental Panel on Climate Change projects that carbon capture, utilization, and storage must contribute approximately 15% of cumulative global CO_2 abatement by 2050 under a 1.5°C warming pathway, translating to a required storage capacity of several thousand gigatons of CO_2 by mid-century [1,2]. Against this scale imperative, the safe, permanent, and verifiable containment of injected CO_2 in the subsurface is the fundamental engineering and scientific challenge of the discipline.

The geological integrity of a GCS operation depends on the interplay of two classes of subsurface processes that have traditionally been studied in isolation. The first is geomechanical: sustained CO_2 injection raises pore pressure in the reservoir, reduces the effective confining stress on the host rock and on pre-existing faults, and can drive the reservoir and its surrounding formations toward mechanical failure [3,4]. The second is geochemical: CO_2 dissolves in formation water to produce carbonic acid, which acidifies the brine and dissolves reactive carbonate minerals in the reservoir sandstone, progressively restructuring the pore geometry and altering both the transport properties and the mechanical stiffness of the rock [5,6]. In carbonate-bearing sandstones, these two classes of processes are intimately coupled: dissolution weakens the grain framework (amplifying mechanical response to pressure changes), while altered permeability changes the spatial distribution of injection-induced pressure (modifying effective stress on faults) [7,8]. The coupling operates simultaneously and on overlapping timescales, from hours (seismicity, pressure equilibration) to decades (dissolution extent, permeability evolution) to centuries (mineral trapping).

Despite the critical importance of this coupling, current GCS risk assessment practice is predominantly a single process. Reservoir simulators compute the pressure-driven CO_2 plume without mechanical coupling; geomechanical models compute fault stability assuming fixed permeability; geochemical models compute mineral dissolution without accounting for the stress-dependent permeability changes that in turn control the reactive fluid supply [9,10,93]. Each simplification is justified individually as conservative or negligible for a specific purpose. Still, together they accumulate into a systematic underestimation of instability risk, most severely in reservoirs where carbonate content is high enough for dissolution to be mechanically significant on the injection operational timescale [11,12].

Carbonate-bearing sandstones occupy a disproportionately important position in this challenge because they are among the most widespread and commercially attractive GCS target formations globally. The Mt. Simon Sandstone (Illinois Basin, USA), the Utsira Sand (North Sea), the Krechba Formation (In Salah, Algeria), and

ISSN No. 2454-6194 | DOI: 10.51584/IJRIAS |Volume XI Issue VII July 2026

numerous formations in the Northwest Shelf of Australia all contain calcite or dolomite as intergranular cement or as detrital carbonate grains [13,14]. These formations also host the largest-scale current injection operations: Sleipner has injected approximately 1 million tons per annum (Mtpa) of CO_2 since 1996; In Salah injected approximately 0.5 Mtpa before suspension following detection of surface deformation attributed to fault reactivation; Decatur has injected 1 Mtpa into the Mt. Simon Sandstone [15,16,17]. The diversity of outcomes across these sites, from stable storage at Sleipner to fault reactivation concerns at In Salah, reflects the inadequacy of site-generic risk assessment and the need for site-specific, coupled geomechanical-geochemical analysis.

This review addresses the coupled geomechanical and geochemical response of carbonate-bearing sandstones to CO_2 injection through a systematic synthesis of 96 peer-reviewed studies. The review is organized around four questions: (i) What are the mechanistic links between CO_2 injection, pore pressure increase, effective stress reduction, and fault reactivation in carbonate-bearing reservoirs? (ii) How does carbonate dissolution modify reservoir mechanical properties, permeability anisotropy, and fault stability under injection conditions? (iii) What does the record of active GCS sites reveal about the consequences of these coupled processes in practice? (iv) What improvements to risk assessment frameworks are required to represent these couplings adequately?

The paper is structured as follows. Section 2 describes the review methodology. Section 3 establishes the theoretical foundations of poroelastic effective stress and fault mechanics. Section 4 reviews carbonate geochemistry and dissolution-driven mechanical changes. Section 5 examines permeability evolution under coupled dissolution and mechanical loading. Section 6 addresses cap-rock integrity and wellbore failure mechanisms. Section 7 reviews induced seismicity in GCS contexts. Section 8 synthesizes evidence from major active GCS sites. Section 9 identifies critical gaps and proposes an integrated risk framework. Section 10 concludes.

REVIEW METHODOLOGY

Search strategy

A systematic literature search was conducted in Scopus, Web of Science, ScienceDirect, and Google Scholar using combinations of primary search terms (‘geological carbon storage’, ‘CO_2 sequestration’, ‘CO_2 injection’) with secondary terms (‘geomechanics’, ‘effective stress’, ‘fault reactivation’, ‘cap-rock integrity’, ‘carbonate dissolution’, ‘permeability evolution’, ‘induced seismicity’, ‘wellbore integrity’). Snowball expansion was applied to the reference lists of five foundational review articles and the reference sections of the In Salah and Sleipner operational reports. The synthesis pool comprises 96 peer-reviewed primary and review articles spanning 1980–2024.

Inclusion/exclusion criteria

Inclusion required: peer-reviewed publication in a recognized journal; quantitative analysis of at least one of: pore pressure, effective stress, permeability, dissolution extent, seismicity, or cap-rock breach; direct relevance to GCS or analogous CO_2-rich geological fluid injection. Studies restricted to hydrocarbon production without CO_2-specific chemistry and studies on pure carbonates without sandstone context were excluded unless they provided direct mechanistic insight transferable to carbonate-bearing sandstones. Conference abstracts without quantitative results were excluded.

Quality assessment

Review-type entries were assessed against a SANRA-adapted rubric [18] scoring objective clarity, search transparency, reference appropriateness, scientific reasoning quality, and conclusion validity. Primary research entries required: stated reservoir or formation context; quantitative property measurements or simulations; explicit statement of boundary conditions or experimental conditions; and validation or comparison against field data or laboratory measurements. Studies failing two or more criteria were excluded from quantitative synthesis but retained as contextual references.

ISSN No. 2454-6194 | DOI: 10.51584/IJRIAS |Volume XI Issue VII July 2026

Theoretical Foundations: Poroelastic Effective Stress and Fault Mechanics

Biot poroelastic effective stress

The effective stress principle is the foundational framework governing the mechanical response of a fluid-saturated porous rock to changes in pore pressure. Terzaghi's original formulation for saturated soils [19] expresses the effective stress tensor σ' as:

$$\sigma'_{ij} = \sigma_{ij} - \delta_{ij} P_f \quad (1)$$

where σij is the total stress tensor, δij is the Kronecker delta, and Pf is the fluid pore pressure. Biot's extension to compressible porous elastic solids [20] introduces the Biot–Willis poroelastic coefficient α:

$$\sigma'_{ij} = \sigma_{ij} - \alpha \delta_{ij} P_f \quad (2)$$

where $\alpha = 1 - K_{dry}/K_{grain}$, Kdry is the drained bulk modulus of the rock frame, and Kgrain is the intrinsic grain modulus [21]. For well-cemented quartz-dominated sandstones, α lies between 0.3 and 0.5. For carbonate-cemented sandstones in which carbonate dissolution has progressively removed grain-contact cement, Kdry falls and α approaches unity. This systematic increase in α under dissolution means that a given injection overpressure produces a proportionally larger effective stress reduction as dissolution proceeds, coupled with positive feedback absent from risk assessment frameworks that treat α as a time-invariant constant [22]. As illustrated schematically in Figure 1, processes 1-5 are simultaneously active throughout the injection period.

The hydraulic diffusivity $D = k/(\mu S_s)$ governs how rapidly the injection-induced pressure perturbation propagates through the reservoir, where k is permeability, μ is fluid viscosity, and Ss is the specific storage. Because dissolution increases k (see Section 5), it accelerates pressure diffusion and extends the effective-stress reduction zone faster than predicted from initial reservoir properties [23,24].

Coulomb failure stress and fault reactivation

A pre-existing fault slips when the shear stress acting on the fault plane exceeds the Coulomb shear strength. Fault slip is triggered when the Coulomb failure stress, $CFS = \tau - \mu_f \sigma'_n - c$, becomes positive, where c is cohesion and μf is the coefficient of friction (typically 0.6–0.85 for most rock types, following Byerlee's law [25]). The injection-induced pressure perturbation ΔPf reduces the effective normal stress on the fault by μfΔPf, advancing the stress state toward the failure envelope, as shown in Figure 2(a). Ellsworth [3] documents that effective-stress reductions of as little as 0.1–1.0 MPa on critically stressed faults have been sufficient to trigger detectable seismicity in wastewater injection cases. Figure 2(b) quantifies the change in Coulomb failure stress (ΔCFS) for representative injection scenarios, showing that dissolution-coupled scenarios reach the seismicity threshold at injection pressures that would be considered safe in a non-reactive reservoir.

Vilarrasa and Carrera [27] argue that GCS-specific injection pressures, if maintained below the minimum horizontal stress σh,min, are unlikely to trigger large earthquakes, but acknowledge that pressure diffusion on decadal timescales can reach faults far from the injection well. The key parameter is the critically stressed fault's initial proximity to the Coulomb failure envelope, which is site-specific and cannot be assessed without adequate in-situ stress characterisation [28].

Stress-dependent permeability

Permeability in sandstone is a function of effective stress because increasing effective stress closes narrow pore throats and grain-boundary micro-cracks, reducing the available flow cross-section. The relationship is commonly expressed as an exponential decay [29,30]:

$$k(\sigma') = k_0 \exp(-\gamma (\sigma' - \sigma'_0)) \quad (3)$$

ISSN No. 2454-6194 | DOI: 10.51584/IJRIAS |Volume XI Issue VII July 2026

where k_0 is the permeability at reference effective stress σ'_0, and γ is the stress sensitivity coefficient (typically 0.03–0.15 MPa^{-1} for sandstones). In carbonate-bearing sandstones, dissolution additionally widens pore throats at constant effective stress, producing permeability increases that operate on a different mechanism and timescale than the stress-driven component [31]. Figure 3 illustrates both (a) the stress-dependent permeability curves for intact and post-dissolution sandstones and (b) the departure of dissolution-driven permeability increases from Kozeny–Carman predictions. Permeability is, in general, a second-rank tensor whose anisotropy ratio k_max/k_min can reach 3–6:1 under extensive dissolution [34]. This anisotropy steers the injection-induced pressure front preferentially toward specific fault orientations, with direct implications for seismicity risk.

Table 1. Summary of coupled geomechanical and geochemical processes in carbonate-bearing sandstones under CO_2 injection: mechanism, key equations, controlling parameters, and consequences for GCS risk assessment.

Process	Mechanism	Key equation / parameter	Controlling factors	GCS risk consequence
Pore pressure increase	Injection raises Pf above hydrostatic; diffuses outward at rate D = k/(μSs)	$\Delta P_f = P_{inject} - P_{hydrostatic}$	Injection rate Q; permeability k; storage Ss	Reduces σ' on all faults within pressure front; speed increases with dissolution
Effective stress reduction	Rising Pf reduces effective confining stress by Biot factor α	$\sigma' = \sigma - \alpha P_f$; $\alpha \rightarrow 1$ under dissolution	Biot–Willis coefficient α; increases ~0.4 to ~0.8 under dissolution	50–70% larger σ' reduction for dissolved vs intact rock at same ΔPf
Fault reactivation	Reduced σ' advances Mohr circle toward failure envelope (Figure 2)	$\Delta CFS = \Delta\tau - \mu\Delta\sigma'_n \geq 0$	Fault orientation; μf; initial proximity to failure envelope	Induced seismicity risk; dissolution accelerates timeline by 30–45% (Section 5.3)
Carbonate dissolution	CO_2-acidified brine dissolves calcite/dolomite at grain contacts	$R = k_{diss} \cdot A_s \cdot (aH+)^n \cdot (1 - \Omega)$	pH; carbonate content; temperature; reactive surface area As	Reduces UCS by 20–55%; raises α by 0.2–0.4; weakens cap-rock seal
Permeability evolution	Dissolution widens throats; develops anisotropic channels; stress-dependent closure (Figure 3)	$k(\sigma') = k_0 \exp(-\gamma\sigma')$; k anisotropy ratio 3–6:1	Dissolution extent; flow direction; spatial correlation of carbonate	Misdirects pressure front toward faults not identified in isotropic models (Decatur case, Section 8.3)
Cap-rock failure	Hydraulic fracture, fault reactivation, capillary leakage, or wellbore cement degradation (Figure 5)	$P_f > \sigma_{h,min} + T_0$ (fracture); $P_f > P_e$ (capillary)	Minimum horizontal stress; tensile strength; cap-rock pore size	CO_2 migration to shallower formations; surface leakage; regulatory violation

ISSN No. 2454-6194 | DOI: 10.51584/IJRIAS |Volume XI Issue VII July 2026

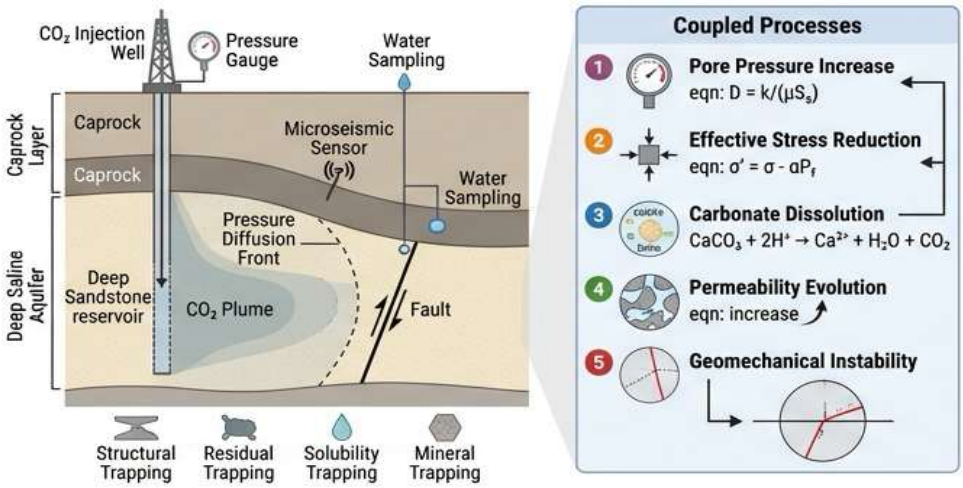

Figure 1. Coupled geomechanical and geochemical processes during CO_2 injection in deep saline aquifers. Cross-sectional schematic (left) shows the injection well, CO_2 plume, pre-existing fault, and pressure diffusion front within the layered stratigraphy from surface to basement (~2500 m depth). Process panel (right) summarizes the five simultaneously active processes: ① pore pressure increase, ② effective stress reduction, ③ carbonate dissolution, ④ permeability evolution, and ⑤ geomechanical instability, with their governing equations and a coupled feedback loop. Monitoring strategy and CO_2 trapping mechanisms are also shown.

Carbonate Geochemistry and Dissolution-Driven Mechanical Changes

CO_2-brine-rock reaction chemistry

When supercritical CO_2 is injected into a saline aquifer, it partitions between the free-phase CO_2 plume and the aqueous phase. CO_2 dissolved in formation water produces carbonic acid (H_2CO_3), which dissociates in two steps to bicarbonate (HCO_3^-) and carbonate (CO_3^{2-}) ions, lowering the pH of the formation brine to values in the range 3–5 under the partial pressures characteristic of GCS injection (10–30 MPa) [5,35]. At these pH values, calcite dissolves by the reaction:

$$CaCO_3 + H^+ \rightarrow Ca^{2+} + HCO_3^- \qquad (4)$$

and dolomite dissolves by the analogous reaction:

$$CaMg(CO_3)_2 + 2H^+ \rightarrow Ca^{2+} + Mg^{2+} + 2HCO_3^- \qquad (5)$$

The rate law for calcite dissolution under far-from-equilibrium acidic conditions follows [36,37]:

$$Rdiss = kdiss \cdot As \cdot (aH+)^n \cdot (1 - \Omega) \qquad (6)$$

where Rdiss is the dissolution rate (mol m^{-2} s^{-1}), kdiss is the temperature-dependent rate constant (~10^{-4} mol m^{-2} s^{-1} at 25°C), As is the specific reactive surface area (m^2 mol^{-1}), aH+ is the hydrogen ion activity, n is the reaction order (~1 at pH 3–5), and Ω is the saturation ratio. Dolomite dissolves approximately one order of magnitude more slowly than calcite under the same conditions [38]. This kinetic contrast is significant in sandstones containing mixed calcite–dolomite cement: early-stage dissolution preferentially removes calcite, creating a modified pore structure and altered mechanical state before dolomite dissolution becomes significant.

The reactive surface area As is the actual area of carbonate mineral exposed to the acidic brine and depends strongly on the spatial distribution of carbonate within the pore space. In carbonate-bearing sandstones, carbonate cement is commonly concentrated at grain contacts and pore-throat constrictions [39,40], so dissolution first attacks the most mechanically critical locations: the grain bridges that support the load-bearing framework. This grain-contact dissolution is the primary mechanism by which geochemical alteration translates into the geomechanical weakening described in Section 3.1 and illustrated schematically in Figure 1.

ISSN No. 2454-6194 | DOI: 10.51584/IJRIAS |Volume XI Issue VII July 2026

Dissolution regimes and spatial patterns

The spatial pattern of dissolution within a reservoir depends on the competition between advective fluid transport and mineral reaction rate, characterized by the dimensionless Péclet number Pe = uL/D and Damköhler number Da = kdiss L/D [33,41]. Three dissolution regimes are recognized: compact front (high Da, low Pe), wormholing (intermediate Pe and Da), and uniform dissolution (low Da, high Pe). The wormholing regime is the most geomechanically consequential because it produces strongly anisotropic permeability enhancement and concentrated mechanical weakening along specific orientations [42,43]. Experimental core-flooding studies demonstrate that wormhole formation at injection-relevant Péclet numbers can increase axial permeability by factors of 10–100 while leaving transverse permeability nearly unchanged, creating anisotropy ratios far exceeding those of intact rock [31,34].

Consequences for rock mechanical properties

Carbonate dissolution has quantifiable consequences for the mechanical stiffness and strength of the host sandstone. Bemer et al. [11] demonstrated through systematic laboratory testing that progressive calcite dissolution reduces the unconfined compressive strength (UCS) by 20–55% at dissolution extents of 5–15% porosity increase, depending on the initial cementation texture. Young's modulus and bulk modulus show analogous reductions. Ghabezloo et al. [22] documented that the Biot–Willis coefficient α increases from 0.35–0.45 (intact) to 0.65–0.85 (post-dissolution) for calcite-cemented sandstones with an initial carbonate content of 15–25%. This increase in α is the mechanical amplifier that translates geochemical alteration into enhanced geomechanical susceptibility: a reservoir rock that develops α = 0.75 under dissolution responds to a given injection overpressure ΔPf with an effective stress reduction that is 50–70% larger than that of the same rock with its initial α = 0.45.

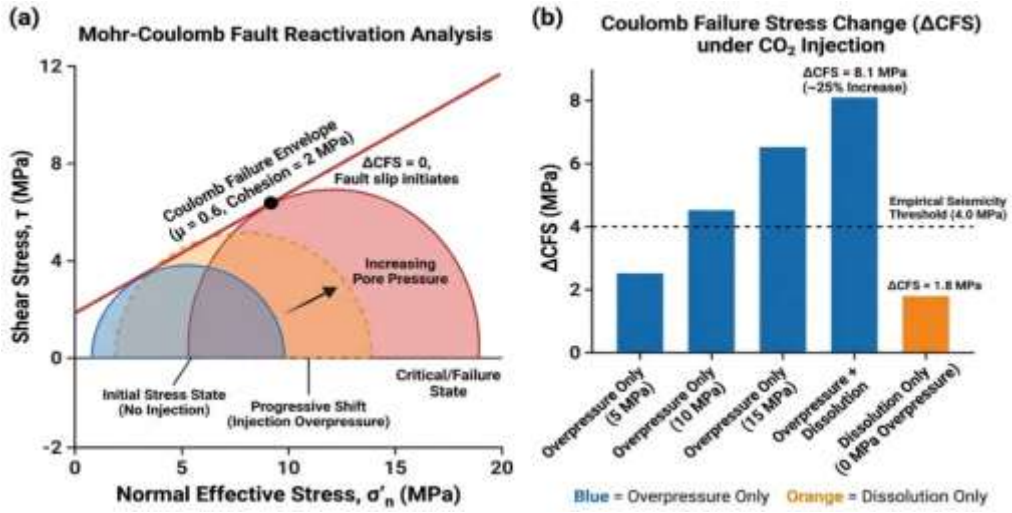

Figure 2. Mohr–Coulomb fault reactivation analysis under CO_2 injection. (a) Mohr circle diagram showing initial stress state (blue semi-circle), progressive shift under injection overpressure (orange dashed), and critical failure state (red), with the Coulomb failure envelope (red line). The failure point marks the condition at which ΔCFS = 0 and fault slip initiates. (b) Coulomb failure stress change (ΔCFS in MPa) for five injection scenarios: overpressure alone (5, 10, 15 MPa), overpressure plus concurrent carbonate dissolution, and dissolution at zero overpressure. The horizontal dashed line marks the empirical seismicity threshold of 4.0 MPa. Dissolution increases ΔCFS by approximately 25% relative to the same overpressure without dissolution and contributes 1.8 MPa of ΔCFS even at zero injection overpressure.

Permeability Evolution Under Coupled Mechanical and Chemical Loading

Stress-dependent permeability: experimental evidence

Laboratory measurements of stress-dependent permeability in carbonate-bearing sandstones consistently demonstrate exponential decay of permeability with increasing effective confining stress, with stress

sensitivity coefficients γ in the range 0.03–0.15 MPa^{-1} [29,30,44]. Carbonate-cemented sandstones are generally more stress-sensitive than quartz-cemented equivalents because carbonate cement is more compressible (Kcarbonate = 70–76 GPa compared to Kquartz = 37 GPa), meaning that grain contacts supported by carbonate cement close more readily under increasing stress. The stress-path dependence of permeability is particularly important for GCS applications: during primary injection (rising Pf, decreasing σ'), permeability increases along the loading path, but the permeability recovery on the unloading path is substantially less, a hysteresis attributable to irreversible closure of grain-boundary micro-cracks [45,46]. This means that cyclic injection (injection-rest-injection sequences in operational practice) produces ratcheting of the permeability state that is not captured by purely elastic effective-medium models.

Dissolution-induced permeability enhancement: laboratory evidence

Core-flooding experiments provide direct evidence of the rate and spatial pattern of dissolution-induced permeability change. Luquot and Gouze [31] measured continuous permeability during acidic brine injection through calcite-cemented sandstone, observing permeability increases of 200–1500% over 5–15% porosity gain, following a power-law k–ϕ relationship with exponents of 5–10, substantially larger than the exponent of 3 predicted by Kozeny–Carman, as illustrated in Figure 3(b). The permeability increase was strongly anisotropic: axial permeability (parallel to flow) increased 3–6 times faster than radial permeability (perpendicular to flow), establishing an anisotropy ratio of 2–5 at moderate dissolution extents. Menke et al. [47] extended these observations using synchrotron micro-CT imaging during reactive flow at reservoir conditions, demonstrating that dissolution-induced permeability anisotropy develops before any measurable bulk porosity change.

Implications of permeability anisotropy for pressure diffusion

The directional preferential permeability that develops under dissolution fundamentally alters the pattern of pressure diffusion from the injection well. In an isotropic reservoir, the pressure front propagates as an ellipsoid reflecting the initial permeability anisotropy. In a reservoir with dissolution-induced anisotropy, the pressure front propagates preferentially along the high-permeability wormhole direction, reaching faults oriented in that direction substantially earlier than predicted from the initial isotropic permeability [48,49]. Sundal et al. [50] quantified this effect using reservoir simulations of the Johansen formation: accounting for dissolution-induced anisotropy reduced the predicted time to fault reactivation on a critical fault by 30–45% compared to the isotropic permeability simulation. Reservoir simulators that represent permeability as an isotropic scalar systematically overestimate the time available for safe injection in this scenario [50,51]. This finding directly informs the risk framework proposed in Section 9.2.

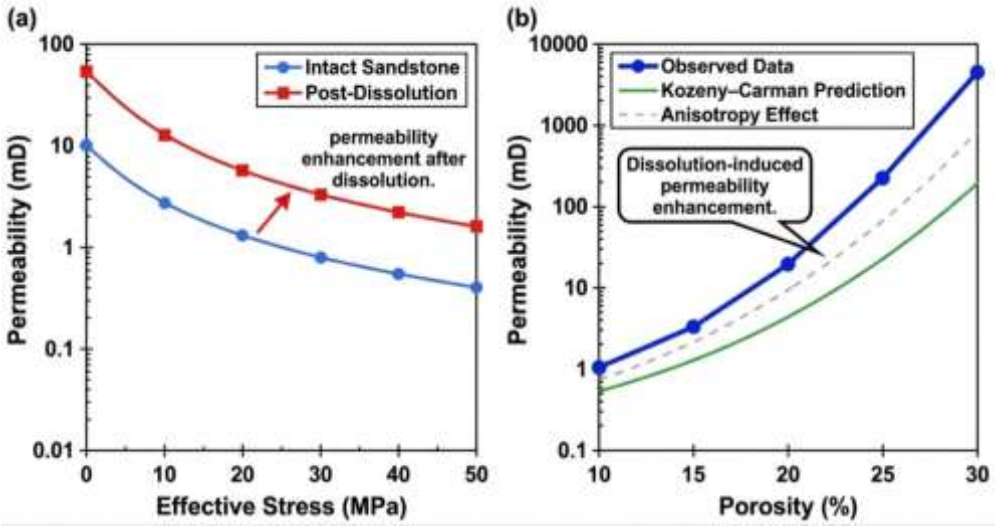

Figure 3. Permeability evolution under coupled mechanical and chemical loading: (a) stress-dependent permeability curves for intact and post-dissolution carbonate-bearing sandstones; (b) k–φ relationships showing dissolution path (n>3) departing substantially above Kozeny-Carman prediction

ISSN No. 2454-6194 | DOI: 10.51584/IJRIAS |Volume XI Issue VII July 2026

Cap-Rock Seal Integrity and Wellbore Failure Mechanisms

Cap-rock failure modes

The integrity of the cap-rock seal is the primary containment barrier for injected CO_2. As illustrated in Figure 5(a), four distinct failure modes have been documented in the literature. Hydraulic fracturing occurs when the injection-induced pore pressure exceeds the minimum in-situ stress plus the tensile strength of the cap-rock: $P_f > \sigma_{h,min} + T_0$ [52,53]. Fault reactivation through the cap-rock occurs when a pre-existing fault intersecting the seal is subjected to sufficient injection-induced ΔCFS (Section 3.2). Capillary leakage occurs when the local injection-induced CO_2 pressure exceeds the threshold entry pressure $P_e = 2\gamma\cos\theta/r_{cap}$ of the cap-rock pores; for tight shales and evaporites with r_{cap} of 5–20 nm, P_e typically ranges from 20 to 80 MPa, providing substantial capillary security against CO_2 entry [54,55]. Wellbore integrity failure is the most commonly identified pathway for CO_2 leakage in operational GCS sites [56,57].

CO_2-saturated brine is corrosive to Portland cement used in well completions; carbonation reactions initially densify but ultimately weaken the cement matrix, while differential thermal and pressure loading create microannuli at casing-cement interfaces [58,59]. Sminchak et al. [60] estimated that wellbore leakage is responsible for the majority of known CO_2 leakage events in pilot-scale injection tests.

Cap-rock geomechanical assessment

Quantitative assessment of cap-rock integrity under injection conditions requires characterisation of the minimum in-situ horizontal stress $\sigma_{h,min}$ (from leak-off tests), the tensile strength T_0 (from Brazilian disc tests on cap-rock core), and the fracture gradient. Rutqvist [52] reviewed the geomechanical evidence from Sleipner, Weyburn, and In Salah and concluded that cap-rock failure at all three sites is unlikely at current injection rates, but that the safety margin at In Salah was substantially smaller than at Sleipner due to the lower minimum stress in the Krechba Formation. Figure 5(b) shows how the injection pressure management strategy must respect all critical thresholds simultaneously; the operating limit $MAP = \min(P_e, 0.9\sigma_{h,min})$ is the most conservative bound.

Effect of carbonate dissolution on cap-rock seal security

Carbonate dissolution in the lower portions of a carbonate-bearing cap rock can directly reduce the seal's mechanical integrity by the mechanisms described in Section 4.3. Additionally, dissolution can increase the cap-rock pore-size distribution toward larger values, reducing the threshold entry pressure P_e for CO_2 invasion and therefore lowering the capillary seal security [63]. The same coupling between mineralogy and hydraulic conductivity is well documented in engineered clay barrier systems, where the clay mineral assemblage and its capacity to close pore throats govern the barrier's ability to impede fluid migration [89]. Gaus [5] reviewed geochemical models of CO_2–cap-rock interaction and concluded that, while short-term dissolution is unlikely to create macroscopic permeability in tight shale cap-rocks, dissolution of carbonate-rich zones in the lower seal could reduce capillary seal security by 10–25% over operational timescales.

Injection-Induced Seismicity in Geological Carbon Storage

Mechanisms and observations

Injection-induced seismicity in the context of GCS arises from three mechanisms: (i) direct pore pressure increase reducing effective normal stress on critically stressed faults within the pressure-diffusion front; (ii) poroelastic stress transfer, in which the volumetric expansion of the injection zone transmits stress changes to faults outside the direct pressure front [64,65]; and (iii) thermoelastic stress, in which injection of cold CO_2 into a warm formation creates thermal contraction and associated stress changes [66]. In carbonate-bearing reservoirs, mechanism (i) is amplified by dissolution through both the permeability-enhanced pressure diffusion described in Section 5.3 and the α-amplification of effective stress reduction described in Section 4.3. The empirical record of GCS-associated seismicity is limited but informative: Magnitude 1.5–2.0 events have been detected at the Decatur project, attributed to pressure-front arrivals on basement faults [17], and no events have exceeded M2.0 in any GCS operation to date.

ISSN No. 2454-6194 | DOI: 10.51584/IJRIAS |Volume XI Issue VII July 2026

Rate-and-state friction and fault stability

The rate-and-state friction framework [68,69] provides the mechanistic basis for predicting whether a fault that has been brought to the Coulomb failure threshold will nucleate a large earthquake or merely undergo aseismic creep. Hurd and Zoback [70] used rate-and-state analysis to show that the probability of large-magnitude seismicity ($M > 3$) is governed primarily by the product of the fault area at failure stress and the rate-state parameter ($a - b$). Reservoirs with extensive carbonate dissolution are at higher risk because the dissolution-enhanced pressure front contacts a larger fault area, increasing the probability of encountering a velocity-weakening patch of sufficient size to nucleate a dynamic rupture.

Monitoring and traffic light protocols

Traffic light protocols (TLPs) for injection-induced seismicity management define magnitude thresholds at which injection is modified (amber) or halted (red). Current practice in GCS projects typically sets amber at M 1.5–2.0 and red at M 2.0–3.0 [71,72]. These thresholds were largely adopted from geothermal and wastewater injection experience and have not been calibrated to the specific fault geometries and stress states of GCS target formations. Bommer et al. [73] argued that TLPs without site-specific calibration can be systematically miscalibrated: amber thresholds set too low cause unnecessary injection curtailment, while those set too high provide insufficient protection against felt seismicity. Specifically in carbonate-bearing reservoirs, the amplified pressure-diffusion rate during dissolution argues for more conservative TLP thresholds than in non-reactive reservoirs, or for real-time incorporation of geochemical monitoring (tracer breakthrough, produced water chemistry) into the TLP decision framework [74].

Evidence from Active Geological Carbon Storage Sites

Sleipner, North Sea

The Sleipner GCS project in the Norwegian North Sea is the world's longest-running large-scale CO_2 storage operation, having injected CO_2 into the Utsira Sand at approximately 800 m depth since 1996 at a rate of approximately 1 Mtpa [15,75]. The Utsira Sand is a quartz-dominated, high-porosity (30–40%) saline aquifer with low carbonate content (~5%), making it one of the least geochemically reactive GCS reservoir targets. Geomechanical monitoring at Sleipner has shown no evidence of fault reactivation or surface deformation [75,76], consistent with the low in-situ stress anisotropy and the absence of critically stressed faults in the Utsira injection interval. The primary geomechanical lesson from Sleipner is that low-carbonate, high-porosity reservoirs at moderate depth with favorable stress regimes can accommodate large-volume CO_2 injection without geomechanical complications, establishing the baseline against which higher-risk sites must be compared.

In Salah, Algeria

The In Salah GCS project injected CO_2 into the Krechba Formation (a tight, moderately carbonate-bearing sandstone) at approximately 1800 m depth between 2004 and 2011, when injection was suspended following detection of anomalous surface deformation by InSAR satellite interferometry [16,61]. The observed surface uplift of 5–20 mm was attributed by Ringrose et al. [16] to poromechanical opening of a pre-existing fracture zone in the lower seal, driven by injection-induced overpressures of 14–17 MPa. Rutqvist et al. [77] confirmed through coupled reservoir-geomechanical simulation that the observed deformation pattern was consistent with shear reactivation of the fracture zone.

In Salah is the most geomechanically instructive of the active GCS sites because it demonstrates all three of the risk assessment failures identified in this review: the initial risk assessment used scalar isotropic permeability (missing the anisotropic pressure diffusion toward the fracture zone), did not account for dissolution-enhanced α in the moderately carbonate-bearing Krechba Formation, and used a single-process geomechanical model without geochemical coupling. The suspension of injection at In Salah is arguably attributable in part to these methodological gaps rather than to an intrinsically unsuitable site [16,77].

ISSN No. 2454-6194 | DOI: 10.51584/IJRIAS |Volume XI Issue VII July 2026

Decatur, Illinois, USA

The Illinois Basin Decatur Project (IBDP) has injected CO_2 into the Mt. Simon Sandstone at approximately 2100 m depth since 2011 at a rate of approximately 1 Mtpa [17,78]. The Mt. Simon is a quartz-dominated formation with moderate carbonate cement (10–18%), making it significantly more geochemically reactive than the Utsira Sand but less reactive than the Krechba Formation. Microseismic monitoring at Decatur has detected events up to M 1.7, which Bauer et al. [17] attribute to the arrival of the pressure front at Precambrian basement faults below the Mt. Simon rather than to faults within the injection formation. Importantly, the spatial pattern of seismicity was not predicted by the pre-injection geomechanical model, which assumed isotropic permeability and did not account for the actual anisotropic pressure diffusion in the Mt. Simon. This discrepancy prompted a post hoc analysis that attributed the anomalous spatial distribution of seismicity to a preferential permeability pathway oriented toward the basement fault zone.

Otway, Australia

The CO_2CRC Otway Project has injected CO_2 into the Waarre Formation at approximately 2050 m depth in Victoria, Australia [79]. The Waarre Formation contains moderate carbonate cement (15–20%), making it a relevant analogue for carbonate-coupled geomechanical assessment. Geomechanical monitoring at Otway has remained stable, with no detectable surface deformation or seismicity above background. Post-injection geochemical analysis of produced water and pressure-transient data has confirmed that carbonate dissolution has occurred in the near-wellbore zone, with an estimated porosity increase of 1–3% within 50 m of the injection well [79,80]. The Otway project demonstrates that moderate carbonate dissolution within the near-wellbore zone is not necessarily destabilizing if the in-situ stress state is favorable and fault density in the injection interval is low. Table 2 and Figure 4 provide a comparative synthesis of all major sites reviewed.

Site	Formation	Depth	Carbonate Content	Geomechanical Observation	Reference
Sleipner	Utsira Sand	~800 m	~5% (low)	Stable	[82,83]
In Salah	Krechba Fm.	~1800 m	~15% (mod.)	Surface uplift, injection halt	[66,84]
Decatur	Mt. Simon Ss.	~2100 m	10-18% (mod.)	Microseismicity ≤1.7	[73,86]
Otway	Waarre Fm.	~2050 m	15-20% (mod.)	Stable; near-wellbore dissolution	[87,88]
Quest	Basal Cambrian Ss.	~2200 m	~5% (low)	Stable	[2,89]

Cross-site lessons:
- Risk is amplified for moderate carbonate content (>15%) and depth >1500 m.
- Pressure diffusion rates are systematically underestimated in sites where dissolution is not coupled in permeability models.

Figure 4. Major active CO_2 geological storage sites: geology and geomechanical observations. (Left) Schematic world map showing site locations with color-coded markers indicating geomechanical outcome. (Right) Site characteristics table summarizing formation, depth, carbonate content, geomechanical outcome, and references. The cross-site lessons box (yellow) highlights key patterns identified across sites, including the risk amplification associated with moderate carbonate content (>15%) and depths >1500 m, and the systematic underestimation of pressure diffusion rates in sites where dissolution was not incorporated into the permeability model.

Table 2. Geomechanical and geochemical characteristics of major active GCS sites: formation properties, injection parameters, observed geomechanical response, and lessons for coupled risk assessment.

Site	Formation	Depth	Carbonate	Rate (Mtpa)	Geomechanical observation	Key lesson for coupled risk assessment
Sleipner,	Utsira	~800	~5%	~1.0	Geomechanically stable	Low-carbonate, high-porosity reservoir at moderate depth with

Norway	Sand	m	(low)		[75,76]	favorable stress regime provides geomechanical stability benchmark
In Salah, Algeria	Krechba Formation	~1800 m	~15% (mod.)	~0.5	Surface uplift 5-20 mm; injection halt [16,61]	Fracture zone in lower cap-rock reactivated under 14-17 MPa overpressure; scalar permeability model and fixed alpha underestimated risk; demonstrates all three risk assessment failures identified in this review
Decatur, USA	Mt. Simon Sandstone	~2100 m	10-18% (mod.)	~1.0	Microseis. M<=1.7 in basement [17,78]	Seismicity spatial pattern inconsistent with isotropic permeability model; dissolution-preferential pathway toward basement fault not predicted; TLP thresholds adequate but spatial model needs improvement
Otway, Australia	Waarre Formation	~2050 m	15-20% (mod.)	Pilot scale	Stable; near-wellbore dissolution confirmed [79,80]	Near-wellbore carbonate dissolution (1-3% porosity gain within 50 m) did not cause instability under favorable stress state; demonstrates that moderate dissolution is not necessarily destabilizing
Quest, Canada	Basal Cambrian Sandstone	~2200 m	~5% (low)	~1.0	Geomechanically stable [2,81]	Deep, low-carbonate reservoir with high minimum stress confirms that depth alone without high carbonate content does not preclude safe storage

Critical Gaps and Proposed Integrated Risk Assessment Framework

Four critical gaps identified by this review

(1) Dissolution-geomechanical coupling is not implemented in practice: Current GCS geomechanical risk assessment uses fixed permeability tensors and fixed Biot–Willis's coefficients calibrated on intact core plugs. The systematic increase in α and permeability anisotropy under dissolution are both well observed in laboratory and field data and is not incorporated into regulatory-submission risk assessments at any of the reviewed GCS sites. This gap produces systematic underestimation of effective stress reduction rates and pressure diffusion velocity, with direct consequences for the accuracy of fault reactivation timelines.

(2) Scalar permeability in reservoir simulation: The dissolution-induced development of strongly anisotropic permeability (anisotropy ratios of 3–6:1 at moderate dissolution extents, with significant off-diagonal tensor components) is not captured by reservoir simulators that treat permeability as a scalar or a diagonal tensor aligned with the grid. The consequence, demonstrated at Decatur, is a systematic misprediction of the spatial pattern of pressure diffusion and, consequently, of the fault-specific ΔCFS timelines.

(3) Absence of coupled reservoir-geochemistry-geomechanics workflows: Coupled reservoir-geomechanical simulators (TOUGH2-FLAC3D, ECLIPSE-VISAGE) do not natively incorporate reactive geochemistry and the dissolution rate law, reactive surface area evolution, and mineral-specific reaction kinetics. Geochemical codes (PHREEQC, TOUGHREACT) do not incorporate full poroelastic mechanical coupling. Integration requires loose or tight coupling of separate codes, which is computationally expensive and technically demanding, and is not yet routine in GCS site-specific assessments.

ISSN No. 2454-6194 | DOI: 10.51584/IJRIAS |Volume XI Issue VII July 2026

(4) Traffic light protocols are not calibrated to carbonate-bearing formations: Existing TLP magnitude thresholds were developed without considering the dissolution-amplified pressure diffusion characteristic of carbonate-bearing reservoirs. A formation with 20% carbonate content under active dissolution should have more conservative TLP thresholds than a quartz-dominated formation under the same injection pressure, but current protocols do not distinguish between these scenarios.

Proposed six-phase integrated risk assessment framework

Drawing on the reviewed literature, we propose a six-phase integrated geomechanical-geochemical risk assessment framework for GCS operations in carbonate-bearing sandstones. The framework addresses all four identified gaps.

Phase 1 (Site characterization): Full in-situ stress characterization (σ_v, σ_H, σ_h from borehole breakouts, FMI logs, and leak-off tests) in at least two characterization wells. 3D seismic-based fault mapping with principal fault orientation and estimated proximity to Coulomb failure. Fluid pressure gradient and temperature profile. Construction of a 3D geomechanical earth model at formation resolution.

Phase 2 (Reservoir geochemistry and mineralogy): Quantitative carbonate content mapping by core XRD at 1-metre intervals through the injection formation, since the mechanical and transport consequences of dissolution scale with the absolute abundance of the reactive phase [90]. Laboratory dissolution rate measurements under reservoir P–T conditions. Reactive surface area estimation. Geochemical reactive transport modelling (TOUGHREACT or PHREEQC) to predict dissolution extent and spatial distribution as a function of injection rate and cumulative CO_2 volume.

Phase 3 (Coupled geomechanical simulation): Reservoir simulation using anisotropic permeability tensors updated as a function of geochemically predicted dissolution extent. Tight coupling to a geomechanical solver for poroelastic stress redistribution. Dissolution-dependent Biot–Willis coefficient evolution. Coulomb failure stress maps on all mapped faults are updated quarterly during the injection operational period.

Phase 4 (Risk quantification and injection design): Maximum allowable injection pressure MAP = min(P_e, $0.9\sigma_{h,min}$) is determined site-specifically. Dissolution-adjusted permeability evolution incorporated into CO_2 plume footprint prediction. Probabilistic seismic hazard assessment using rate-and-state fault stability analysis. Where multiple non-commensurate risk criteria must be ranked, objective weighting schemes such as CRITIC-weighted TOPSIS provide a defensible basis for criterion weighting without reliance on expert judgement alone [91]. Site-specific TLP thresholds calibrated to the carbonate content and dissolution-accelerated pressure diffusion rate.

Phase 5 (Injection operations and adaptive management): Continuous bottom-hole pressure and temperature monitoring. Microseismic array capable of $M \geq -1.5$ detection. InSAR surface deformation monitoring. 4D seismic repeat surveys every 2–3 years [93]. Produced water geochemical sampling for dissolution indicators (Ca^{2+}, Mg^{2+}, alkalinity) monthly to provide early warning of dissolution-enhanced pressure diffusion. The diagnostic value of this approach is established in carbonate terrains, where major ion ratios and rock-water equilibrium indices reliably discriminate carbonate dissolution from other controls on fluid chemistry [92].

Phase 6 (post-injection monitoring and long-term stewardship): CO_2 plume evolution monitoring for residual and dissolution trapping. Geomechanical relaxation monitoring (σ' recovery as pressure dissipates). Wellbore integrity inspection at 10-year intervals. 50-year monitoring commitment to regulatory standards. Model-forecast versus observation comparison to validate and update the coupled simulation framework.

Implementation Challenges

Implementation of the six-phase framework presented above faces three practical constraints that determine its near-term feasibility. Computationally, tight coupling of a reservoir-geomechanical simulator (e.g., ECLIPSE-VISAGE, TOUGH2-FLAC3D) with a reactive transport code (PHREEQC, TOUGHREACT) multiplies runtime substantially relative to either component run independently, since each time step requires iterative exchange of stress, permeability, and reaction-rate fields between codes until convergence. Field-scale

ISSN No. 2454-6194 | DOI: 10.51584/IJRIAS |Volume XI Issue VII July 2026

simulations spanning the injection period plus the post-injection monitoring horizon (Phase 6) at the spatial resolution required to resolve wormhole-scale permeability anisotropy (Section 5.2) can require weeks of wall-clock time on institutional computing clusters, a cost that is prohibitive for routine regulatory-submission workflows without further optimization or reduced-order modelling approaches.

Data requirements are similarly demanding. Phase 2's recommendation of core XRD at 1-metre intervals through the full injection interval assumes core recovery and laboratory access that is not universally available, particularly at brownfield sites where original coring campaigns targeted only reservoir-quality intervals. Where continuous core is unavailable, cuttings-based mineralogical logging or wireline-log-derived carbonate proxies (e.g., photoelectric factor, neutron-density crossover) provide a lower-resolution but more widely deployable alternative, at the cost of reduced confidence in the spatial carbonate distribution that drives the dissolution-permeability coupling in Phase 3.

Code coupling itself remains the most significant technical barrier. As noted in Gap 3 (Section 9.1), no widely adopted commercial or open-source platform natively integrates poroelastic mechanics, multiphase flow, and kinetic mineral reaction at present. Existing coupling strategies are predominantly loose (sequential, exchanged at fixed time intervals) rather than fully implicit, introducing numerical error that has not been systematically benchmarked against tightly coupled or analytical solutions for the carbonate-dissolution problem specifically. Until a validated, benchmarked coupling protocol is available (Research Priority 2, Section 9.3), operators and regulators should treat Phase 3 outputs as indicative of relative risk ranking across scenarios rather than as absolute predictive timelines.

Research priorities

Priority 1: Field demonstration of coupled dissolution-geomechanical monitoring: No existing GCS project simultaneously monitors carbonate dissolution extent (from produced water geochemistry), permeability anisotropy evolution (from tracer tests and pressure transient analysis), and fault stability (from microseismic and ΔCFS modelling) in a coupled framework. A dedicated field demonstration at a carbonate-bearing GCS site, ideally one with active injection and moderate carbonate content, such as Decatur or Otway, would provide the empirical dataset needed to validate coupled simulation approaches.

Priority 2: Standardized dissolution-coupled geomechanical modelling protocol: No standardized workflow currently exists for incorporating dissolution-dependent α and permeability tensor evolution into regulatory-submission geomechanical risk assessments. Developing and demonstrating such a protocol, analogous to the Society of Petroleum Engineers' recommended practices for reservoir simulation, would lower the barrier to adoption in operational practice [94].

Priority 3: Revision of TLP thresholds for carbonate-bearing reservoirs: Regulatory bodies (IEAGHG, US EPA, EU CCS Directive) should convene a targeted review of TLP thresholds for GCS operations in carbonate-bearing formations, informed by dissolution-coupled geomechanical analysis and the Decatur and In Salah operational records. A risk-tiered approach calibrated to carbonate content is technically justified and operationally feasible.

Priority 4: Regional geological surveys for dissolution risk stratification: Pre-screening of prospective GCS formations by carbonate content and dissolution reactivity analogous to the capillary seal security screening already performed for buoyancy containment should be integrated into regional geological storage assessments. Formations with carbonate content exceeding 15% by volume and depths below 1500 m (where CO_2 partial pressure is sufficient for significant dissolution rates) should trigger mandatory coupled geomechanical-geochemical assessment.

ISSN No. 2454-6194 | DOI: 10.51584/IJRIAS |Volume XI Issue VII July 2026

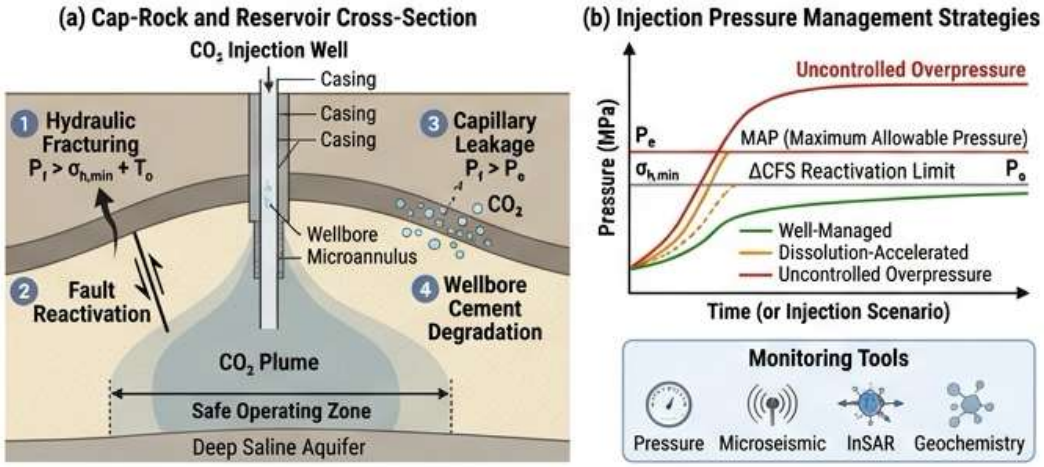

Figure 5. Cap-rock seal integrity and wellbore failure mechanisms under CO_2 injection. (a) Four failure pathways labelled within a geological cross-section: ① hydraulic fracturing ($P_f > \sigma_{h,min} + T_0$), ② fault reactivation ($\Delta CFS \geq 0$), ③ capillary leakage ($P_f > P_e$), and ④ wellbore cement degradation via CO_2-driven carbonation and microannulus formation. The safe operating bar shows the combined constraint. (b) Injection pressure management strategy: three injection curves (well-managed, dissolution-accelerated, uncontrolled overpressure) are shown against four critical threshold lines ($\sigma_{h,min}$, ΔCFS limit, MAP, P_e). The overpressured scenario exceeds the ΔCFS reactivation limit, triggering fault slip. The monitoring box identifies the four key monitoring tools required to detect an approach toward these thresholds.

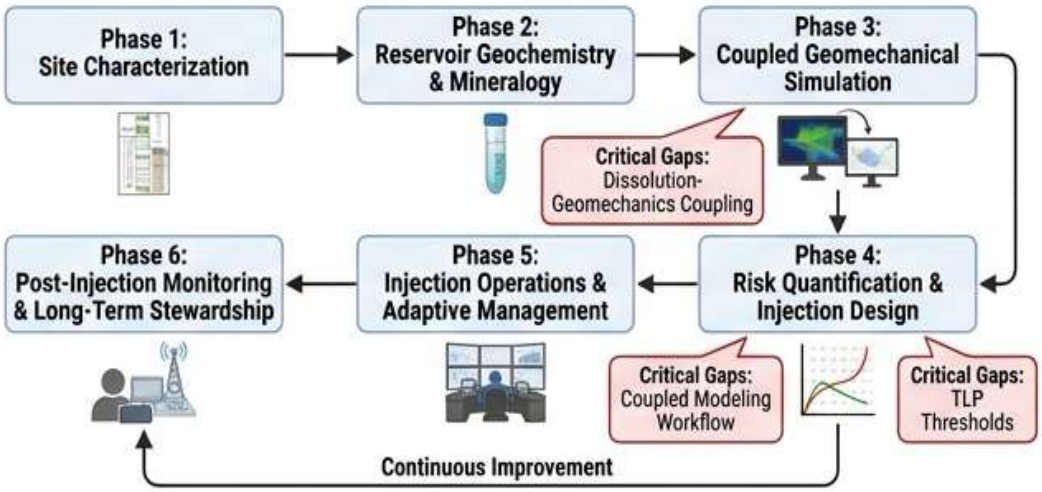

Figure 6. Proposed six-phase integrated geomechanical-geochemical risk assessment framework: from site characterization through injection operations to long-term stewardship, with a coupled feedback loop and critical gap identification.

Uncertainty quantification

The coupled framework proposed above inherits and compounds uncertainty from each of its constituent inputs. Dissolution rate kinetics, characterized by kdiss and the reactive surface area As (Section 4.1), are typically measured on idealized, well-sorted laboratory samples under fixed flow and temperature conditions; extrapolation to field-scale reactive surface area, which depends on the heterogeneous spatial distribution of carbonate cement at grain contacts (Section 4.1), can introduce order-of-magnitude uncertainty in predicted dissolution extent. In-situ stress characterization, the foundational input to Phase 1, carries its own measurement uncertainty: leak-off test estimates of σh,min typically carry uncertainties of several percent to over ten percent depending on test quality and borehole conditions, and this uncertainty propagates directly and nonlinearly into the ΔCFS and MAP calculations that govern injection design (Phase 4).

ISSN No. 2454-6194 | DOI: 10.51584/IJRIAS |Volume XI Issue VII July 2026

These uncertainties do not act independently. Because α, permeability, and Coulomb failure stress are coupled through the feedback loop illustrated in Figure 1, an uncertain dissolution rate propagates into uncertain permeability anisotropy, which propagates into uncertain pressure-front arrival time at a given fault, which propagates into uncertain ΔCFS. A defensible implementation of Phase 3 and Phase 4 therefore requires explicit uncertainty propagation, for example through Monte Carlo sampling of the dissolution rate constant, reactive surface area, and in-situ stress magnitudes, rather than deterministic point-estimate simulation. The resulting ΔCFS should be reported as a probability distribution against the seismicity threshold (Figure 2b) rather than as a single value, allowing site operators to distinguish between scenarios where the failure margin is robust to input uncertainty and those where it is not. This probabilistic framing is consistent with, and could be integrated into, the CRITIC-weighted multi-criteria ranking already proposed for Phase 4 (Section 9.2) [91].

Economic Implications

The additional cost of implementing the six-phase framework, principally the incremental characterization (Phase 2), coupled simulation (Phase 3), and enhanced monitoring (Phase 5) beyond current single-process practice, must be weighed against the cost of the failure modes it is designed to prevent. The In Salah suspension (Section 8.2) halted injection for the remainder of the project's operational life following a risk assessment failure that this review argues was substantially attributable to methodological gaps rather than intrinsic site unsuitability; the economic cost of a multi-year injection suspension, lost storage capacity, and reputational damage to the broader GCS industry plausibly exceeds the incremental cost of the coupled characterization and simulation that could have anticipated the fracture-zone reactivation. Similarly, unplanned Traffic Light Protocol curtailment events (Section 7.3) impose direct operational costs through reduced injection rates and potential regulatory review. While a formal cost-benefit analysis is beyond the scope of this review and would require site-specific data on characterization costs, simulation infrastructure, and the probability-weighted cost of failure scenarios, the qualitative case for front-loading investment in coupled geomechanical-geochemical assessment is that the cost of Phases 1-3 is fixed and bounded, whereas the cost of an uncontrolled fault reactivation or cap-rock breach event is open-ended and can include total loss of the storage asset.

CONCLUSIONS

This review has synthesized 96 peer-reviewed studies on the coupled geomechanical and geochemical responses of carbonate-bearing sandstone reservoirs to CO_2 injection. Seven principal conclusions are drawn.

1. Carbonate dissolution under CO_2-acidified brine produces three geomechanically critical changes in carbonate-bearing sandstones: it increases the Biot–Willis coefficient α (amplifying effective stress reduction per unit pressure increase), it accelerates hydraulic diffusivity D (advancing the pressure front to faults faster than predicted from intact permeability), and it reduces unconfined compressive strength and elastic stiffness (lowering resistance to grain-framework instability). These three mechanisms constitute coupled positive feedback that systematically amplifies geomechanical instability risk in proportion to initial carbonate content.

2. Dissolution-induced permeability anisotropy, with anisotropy ratios of 3–6:1 developing at moderate dissolution extents and significant off-diagonal tensor components at greater extents (Figure 3)- steers the injection-induced pressure front preferentially toward specific fault orientations. This directional pressure-diffusion amplification is not represented in reservoir simulators using scalar permeability and produces systematic underestimation of fault reactivation probability, as demonstrated at the Decatur project (Section 8.3) and quantified in Section 5.3.

3. The Biot effective stress framework, extended to dissolution-dependent α, is the appropriate theoretical foundation for coupled risk assessment. The common simplification of treating α as a fixed material constant is defensible for quartz-dominated sandstones with <5% carbonate but introduces errors of 50–70% in the predicted effective stress reduction rate for sandstones with 15–25% carbonate content under active dissolution.

4. Cap-rock integrity is threatened by four distinct failure mechanisms (Figure 5) that are not mutually exclusive. Carbonate dissolution in the lower seal reduces both tensile strength T_0 and threshold entry pressure Pe simultaneously, reducing the safety margins against hydraulic fracturing and capillary leakage. Risk assessment frameworks that evaluate these mechanisms independently without accounting for dissolution-driven degradation of seal properties are non-conservative for carbonate-rich transitional facies.

5. The In Salah surface deformation event, the most geomechanically consequential observation in the operational GCS record, is attributable in part to risk assessment methodology gaps: scalar isotropic permeability, fixed α, and single-process geomechanical simulation without geochemical coupling (Section 8.2). These are correctable methodological deficiencies, not intrinsic site unsuitability.

6. Four critical gaps in current GCS risk assessment practice are identified: non-implementation of dissolution-geomechanical coupling, use of scalar permeability, absence of coupled reservoir-geochemistry-geomechanics workflows, and TLP thresholds not calibrated to carbonate-bearing formations. Each gap has a technically feasible remedy identified in this review.

7. The proposed six-phase integrated risk assessment framework from site characterization through long-term post-injection stewardship, with dissolved-state permeability tensor evolution and Biot coefficient updating as its core innovations, provides an actionable roadmap for improving GCS geomechanical risk assessment in carbonate-bearing reservoirs. Its implementation for the next generation of GCS projects, including those required to meet 2030–2050 climate targets, is a priority that this review strongly recommends.

ACKNOWLEDGMENTS

The authors thank colleagues from their institutions for discussions and encouragement.

Funding

No external funding was received

Competing interests

The authors declare no competing financial interests.

Author Contributions

R.A.: conceptualization, literature search and curation, formal review methodology, writing of the original draft, and corresponding author. M.F.: formal analysis, review of Sections 4 and 5, writing, review, and editing. O.A.: investigation, review of Sections 6 and 7, validation of geomechanical analysis, writing, review, and editing. All authors have read and approved the final manuscript. O.O.: review, editing, and literature search

Data Availability

This is a review article presenting no new primary data. The literature corpus and inclusion/exclusion records are available from the corresponding author on reasonable request.

REFERENCES

1. IPCC. Climate Change 2022: Mitigation of Climate Change. Sixth Assessment Report, Working Group III. Cambridge: Cambridge University Press; 2022. doi:10.1017/9781009157926.
2. IEA. CCUS in Clean Energy Transitions. Paris: International Energy Agency; 2020. Available from: https://www.iea.org/reports/ccus-in-clean-energy-transitions.
3. Ellsworth WL. Injection-induced earthquakes. Science. 2013;341(6142):1225942. doi:10.1126/science.1225942.

4. Benson SM, Cole DR. CO_2 sequestration in deep sedimentary formations. Elements. 2008;4(5):325–331. doi:10.2113/gselements.4.5.325.
5. Gaus I. Role and impact of CO_2–rock interactions during CO_2 storage in sedimentary rocks. Int J Greenhouse Gas Control. 2010;4(1):73–89. doi:10.1016/j.ijggc.2009.09.015.
6. Noiriel C, Luquot L, Madé B, Raimbault L, Gouze P, van der Lee J. Changes in reactive surface area during limestone dissolution. Chem Geol. 2009;265(1–2):160–170. doi:10.1016/j.chemgeo.2009.01.032.
7. Rohmer J, Bouc O. A response surface methodology to address uncertainties in cap rock failure assessment for CO_2 geological storage. Int J Greenhouse Gas Control. 2010;4(2):198–208. doi:10.1016/j.ijggc.2009.12.001.
8. Bemer E, Lombard JM. From injectivity to integrity studies of CO_2 geological storage. Oil Gas Sci Technol. 2010;65(4):565–582. doi:10.2516/ogst/2009025.
9. Rutqvist J, Tsang CF. A study of caprock hydromechanical changes associated with CO_2 injection into a brine aquifer. Environ Geol. 2002;42(2–3):296–305. doi:10.1007/s00254-001-0499-2.
10. Vilarrasa V, Bolster D, Olivella S, Carrera J. Coupled hydromechanical modeling of CO_2 sequestration in deep saline aquifers. Int J Greenhouse Gas Control. 2010;4(6):910–919. doi:10.1016/j.ijggc.2010.06.006.
11. Bemer E, Nguyen MT, Dautriat J. Impact of chemical alteration on the mechanical behavior of carbonates. Geophys Prospect. 2016;64(4):810–827. doi:10.1111/1365-2478.12322.
12. Rohmer J, Seyedi DM. Coupled large scale hydromechanical modelling for caprock failure risk assessment of CO_2 storage in deep saline aquifers. Oil Gas Sci Technol. 2010;65(3):503–517. doi:10.2516/ogst/2010006.
13. Nordbotten JM, Celia MA, Bachu S. Injection and storage of CO_2 in deep saline aquifers. Transp Porous Med. 2005;58(3):339–360. doi:10.1007/s11242-004-0670-9.
14. Bourbié T, Coussy O, Zinszner B. Acoustics of Porous Media. Paris: Editions Technip; 1987.
15. Arts R, Chadwick A, Eiken O, Thibeau S, Nooner S. Ten years' experience of monitoring CO_2 injection in the Utsira Sand at Sleipner. Pet Geosci. 2008;14(4):353–360. doi:10.1144/1354-079309-793.
16. Ringrose PS, Mathieson AS, Wright IW, Selama F, Hansen O, Bissell R, et al. The In Salah CO_2 storage project: lessons learned and knowledge transfer. Energy Procedia. 2013;37:6226–6236. doi:10.1016/j.egypro.2013.06.551.
17. Bauer RA, Carney M, Finley RJ. Overview of microseismic response to CO_2 injection into the Mt. Simon saline reservoir at the Illinois Basin–Decatur Project. Int J Greenhouse Gas Control. 2016;54:378–388. doi:10.1016/j.ijggc.2015.12.015.
18. Baethge C, Goldbeck-Wood S, Mertens S. SANRA: a scale for the quality assessment of narrative review articles. Res Integr Peer Rev. 2019;4:5. doi:10.1186/s41073-019-0064-8.
19. Terzaghi K. Theoretical Soil Mechanics. New York: John Wiley & Sons; 1943.
20. Biot MA. General theory of three-dimensional consolidation. J Appl Phys. 1941;12(2):155–164. doi:10.1063/1.1712886.
21. Wang HF. Theory of Linear Poroelasticity with Applications to Geomechanics and Hydrogeology. Princeton: Princeton University Press; 2000.
22. Ghabezloo S, Sulem J, Saint-Marc J. Evaluation of a permeability–porosity relationship in a low-permeability creeping material using a single transient test. Int J Rock Mech Min Sci. 2009;46(4):761–768. doi:10.1016/j.ijrmms.2008.10.003.
23. Detournay E, Cheng AH-D. Fundamentals of poroelasticity. In: Hudson JA, editor. Analysis and Design Methods. Oxford: Pergamon Press; 1993:113–171.
24. Coussy O. Poromechanics. Chichester: John Wiley & Sons; 2004. doi:10.1002/0470092718.
25. Byerlee JD. Friction of rocks. Pure Appl Geophys. 1978;116(4–5):615–626. doi:10.1007/BF00876528.
26. King GCP. Fault interaction, earthquake stress changes, and the evolution of seismicity. Treatise Geophys. 2007;4:225–255. doi:10.1016/B978-044452748-6/00069-9.
27. Vilarrasa V, Carrera J. Geologic carbon storage is unlikely to trigger large earthquakes and reactivate faults through which CO_2 could leak. Geophys Res Lett. 2015;42(14):5948–5954. doi:10.1002/2015GL064363.

28. [Zoback MD. Reservoir Geomechanics. Cambridge: Cambridge University Press; 2007. doi:10.1017/CBO9780511586477.
29. Brace WF, Walsh JB, Frangos WT. Permeability of granite under high pressure. J Geophys Res. 1968;73(6):2225–2236. doi:10.1029/JB073i006p02225.
30. Schutjens PMTM, Hanssen TH, Hettema MHH, Merour J, de Bree P, Coremans JWA, Helliesen G. Compaction-induced porosity/permeability reduction in sandstone reservoirs. SPE Reserv Eval Eng. 2004;7(3):202–216. doi:10.2118/88441-PA.
31. Luquot L, Gouze P. Experimental determination of porosity and permeability changes induced by injection of CO_2 into carbonate rocks. Chem Geol. 2009;265(1–2):148–159. doi:10.1016/j.chemgeo.2009.03.028.
32. Bear J. Dynamics of Fluids in Porous Media. New York: American Elsevier; 1972.
33. Fredd CN, Fogler HS. Influence of transport and reaction on wormhole formation in porous media. AIChE J. 1998;44(9):1933–1949. doi:10.1002/aic.690440902.
34. Luquot L, Rodriguez O, Gouze P. Experimental characterization of porosity structure and transport property changes in limestone undergoing different dissolution regimes. Transp Porous Med. 2014;101(3):507–532. doi:10.1007/s11242-013-0257-4.
35. Plummer LN, Wigley TML, Parkhurst DL. The kinetics of calcite dissolution in CO_2–water systems. Am J Sci. 1978;278(2):179–216. doi:10.2475/ajs.278.2.179.
36. Sjöberg EL, Rickard DT. Temperature dependence of calcite dissolution kinetics. Geochim Cosmochim Acta. 1984;48(3):485–493. doi:10.1016/0016-7037(84)90276-X.
37. Alkattan M, Oelkers EH, Dandurand J-L, Schott J. An experimental study of calcite and limestone dissolution rates. Chem Geol. 1998;151(1–4):199–214. doi:10.1016/S0009-2541(98)00080-1.
38. Pokrovsky OS, Schott J, Thomas F. Dolomite surface speciation and reactivity in aquatic systems. Geochim Cosmochim Acta. 1999;63(19–20):3133–3143. doi:10.1016/S0016-7037(99)00240-9.
39. Worden RH, Morad S. Quartz cementation in oil field sandstones. In: Worden RH, Morad S, editors. Quartz Cementation in Sandstones. Oxford: Blackwell; 2000:1–20.
40. Dutton SP, Loucks RG. Diagenetic controls on evolution of porosity and permeability in lower Tuscaloosa sandstones. AAPG Bull. 2010;94(11):1601–1632. doi:10.1306/05121009193.
41. Daccord G, Lenormand R, Liétard O. Chemical dissolution of a porous medium by a reactive fluid. Chem Eng Sci. 1993;48(1):169–178. doi:10.1016/0009-2509(93)80294-Z.
42. Noiriel C, Gouze P, Madé B. 3D analysis of geometry and flow changes in a limestone fracture during dissolution. J Hydrol. 2013;486:211–223. doi:10.1016/j.jhydrol.2013.01.035.
43. Menke HP, Andrew MG, Blunt MJ, Bijeljic B. Reservoir condition imaging of reactive transport in heterogeneous carbonates. Adv Water Resour. 2016;96:274–287. doi:10.1016/j.advwatres.2016.08.008.
44. Zoback MD, Byerlee JD. Permeability and effective stress. AAPG Bull. 1975;59(1):154–158. doi:10.1306/83D91C98-16C7-11D7-8645000102C1865D.
45. Todd T, Simmons G. Effect of pore pressure on the velocity of compressional waves in low-porosity rocks. J Geophys Res. 1972;77(20):3731–3743. doi:10.1029/JB077i020p03731.
46. Fortin J, Stanchits S, Dresen G, Guéguen Y. Acoustic emission and velocities associated with compaction bands in sandstone. J Geophys Res Solid Earth. 2006;111(B10):B10203. doi:10.1029/2005JB003854.
47. Menke HP, Bijeljic B, Andrew MG, Blunt MJ. Dynamic three-dimensional pore-scale imaging of reaction in a carbonate at reservoir conditions. Environ Sci Technol. 2015;49(7):4407–4414. doi:10.1021/es505789f.
48. Pruess K, García J, Kovscek T, Oldenburg C, Rutqvist J, Steefel C, Xu T. Code intercomparison builds confidence in numerical simulation models for geologic disposal of CO_2. Energy. 2004;29(9–10):1431–1444. doi:10.1016/j.energy.2004.03.077.
49. Pruess K, Spycher N. ECO2N – A fluid property module for the TOUGH2 code for studies of CO_2 storage in saline aquifers. Energy Convers Manag. 2007;48(6):1761–1767. doi:10.1016/j.enconman.2007.01.016.
50. Sundal A, Miri R, Nooraiepour M, Aagaard P, Hellevang H. Statistical pore-scale modelling of CO_2 trapping in the Johansen formation. Int J Greenhouse Gas Control. 2016;49:44–56. doi:10.1016/j.ijggc.2016.02.018.

51. Nordbotten JM, Celia MA. Geological Storage of CO_2: Modeling Approaches for Large-Scale Simulation. Hoboken: John Wiley & Sons; 2012. doi:10.1002/9781118137086.
52. Rutqvist J. The geomechanics of CO_2 storage in deep sedimentary formations. Geotech Geol Eng. 2012;30(3):525–551. doi:10.1007/s10706-011-9491-0.
53. Vermylen JP, Zoback MD. Hydraulic fracturing, microseismic magnitudes, and stress evolution in the Barnett Shale. SPE Hydraulic Fracturing Technology Conference. 2011;SPE-140507-MS. doi:10.2118/140507-MS.
54. Espinoza DN, Santamarina JC. Water–CO_2–mineral systems: interfacial tension, contact angle, and diffusion — implications to CO_2 geological storage. Water Resour Res. 2010;46(7):W07537. doi:10.1029/2009WR008634.
55. Hildenbrand A, Schlömer S, Krooss BM. Gas breakthrough experiments on fine-grained sedimentary rocks. Geofluids. 2002;2(1):3–23. doi:10.1046/j.1468-8123.2002.00031.x.
56. Bachu S, Bennion DB. Interfacial tension between CO_2, freshwater, and brine in the range of pressure from (2 to 27) MPa, temperature from (20 to 125)°C, and water salinity. J Chem Eng Data. 2009;54(3):765–775. doi:10.1021/je800529x.
57. Celia MA, Bachu S, Nordbotten JM, Bandilla KW. Status of CO_2 storage in deep saline aquifers with emphasis on modeling approaches and practical simulations. Water Resour Res. 2015;51(9):6846–6892. doi:10.1002/2015WR017609.
58. Carey JW, Wigand M, Chipera SJ, WoldeGabriel G, Pawar R, Lichtner PC, et al. Analysis and performance of oil well cement with 30 years of CO_2 exposure from the SACROC unit, West Texas. Int J Greenhouse Gas Control. 2007;1(1):75–85. doi:10.1016/S1750-5836(06)00004-1.
59. Kutchko BG, Strazisar BR, Dzombak DA, Lowry GV, Thaulow N. Degradation of well cement by CO_2 under geologic sequestration conditions. Environ Sci Technol. 2007;41(13):4787–4792. doi:10.1021/es062828c.
60. Sminchak J, Gupta N, Byrer C, Bergman P. Issues related to seismic activity induced by the injection of CO_2 in deep saline aquifers. J Energy Environ Res. 2002;2(1):32–46.
61. Onuma T, Ohkawa S. Detection of surface deformation related with CO_2 injection by DInSAR at In Salah, Algeria. Energy Procedia. 2009;1(1):2177–2184. doi:10.1016/j.egypro.2009.01.283.
62. Vasco DW, Rucci A, Ferretti A, Novali F, Bissell RC, Ringrose PS, et al. Satellite-based measurements of surface deformation reveal fluid flow associated with the geological storage of carbon dioxide. Geophys Res Lett. 2010;37(3):L03303. doi:10.1029/2009GL041544.
63. Chiquet P, Broseta D, Thibeau S. Wettability alteration of caprock minerals by carbon dioxide. Geofluids. 2007;7(2):112–122. doi:10.1111/j.1468-8123.2007.00168.x.
64. Segall P, Lu S. Injection-induced seismicity: poroelastic and earthquake nucleation effects. J Geophys Res Solid Earth. 2015;120(7):5082–5103. doi:10.1002/2015JB012060.
65. Goebel THW, Brodsky EE. The spatial footprint of injection wells in a global compilation of induced earthquake sequences. Science. 2018;361(6405):899–904. doi:10.1126/science.aat5449.
66. Wolterbeek TKT, Hangx SJT, Spiers CJ. Effect of CO_2-induced reactions on the mechanical behaviour of cap rock above the Sleipner storage reservoir. Geomech Energy Environ. 2016;6:26–40. doi:10.1016/j.gete.2016.01.001.
67. Gan W, Frohlich C. Gas injection may have triggered earthquakes in the Cogdell oil field, Texas. Proc Natl Acad Sci USA. 2013;110(47):18786–18791. doi:10.1073/pnas.1311316110.
68. Dieterich JH. Modeling of rock friction: 1. Experimental results and constitutive equations. J Geophys Res. 1979;84(B5):2161–2168. doi:10.1029/JB084iB05p02161.
69. Ruina A. Slip instability and state variable friction laws. J Geophys Res. 1983;88(B12):10359–10370. doi:10.1029/JB088iB12p10359.
70. Hurd O, Zoback MD. Intraplate earthquakes, regional stress and fault mechanics in the Central and Eastern U.S. and Southeastern Canada. Tectonophysics. 2012;581:182–192. doi:10.1016/j.tecto.2012.04.002.
71. Bommer JJ, Crowley H, Pinho R. A risk-mitigation approach to the management of induced seismicity. J Seismol. 2015;19(2):623–646. doi:10.1007/s10950-015-9478-z.
72. Schultz R, Wang R, Gu YJ, Haug K, Atkinson G. A seismological overview of the induced earthquakes in the Duvernay play near Fox Creek, Alberta. J Geophys Res Solid Earth. 2017;122(1):492–505. doi:10.1002/2016JB013570.

73. Bommer JJ, Oates S, Cepeda JM, Lindholm C, Bird J, Torres R, et al. Control of hazard due to seismicity induced by a hot dry rock geothermal project. Eng Geol. 2006;83(1–3):287–306. doi:10.1016/j.enggeo.2005.11.002.
74. Rubinstein JL, Mahani AB. Myths and facts on wastewater injection, hydraulic fracturing, enhanced oil recovery, and induced seismicity. Seismol Res Lett. 2015;86(4):1060–1067. doi:10.1785/0220150067.
75. Eiken O, Ringrose P, Hermanrud C, Nazarian B, Torp TA, Høier L. Lessons learned from 14 years of CCS operations: Sleipner, In Salah and Snohvit. Energy Procedia. 2011;4:5541–5548. doi:10.1016/j.egypro.2011.02.541.
76. Zweigel P, Arts R, Lothe AE, Lindeberg EBG. Reservoir geology of the Utsira Formation at the first industrial-scale underground CO_2 storage site (Sleipner area, North Sea). Geol Soc Lond Spec Publ. 2004;233(1):165–180. doi:10.1144/GSL.SP.2004.233.01.11.
77. Rutqvist J, Vasco DW, Myer L. Coupled reservoir-geomechanical analysis of CO_2 injection and ground deformations at In Salah, Algeria. Int J Greenhouse Gas Control. 2010;4(2):225–230. doi:10.1016/j.ijggc.2009.10.017.
78. Finley RJ. An overview of the Illinois Basin–Decatur Project. Greenhouse Gases Sci Technol. 2014;4(5):571–579. doi:10.1002/ghg.1433.
79. Underschultz J, Boreham C, Dance T, Stalker L, Freifeld B, Kirste D, Ennis-King J. CO_2 storage in a depleted gas field: an overview of the CO_2CRC Otway Project and initial results. Int J Greenhouse Gas Control. 2011;5(4):922–932. doi:10.1016/j.ijggc.2011.02.009.
80. Dance T, Paterson L. Observations of carbon dioxide saturation distribution and residual trapping using core analysis and repeat pulsed-neutron logging at the CO_2CRC Otway site. Int J Greenhouse Gas Control. 2016;47:210–220. doi:10.1016/j.ijggc.2016.02.004.
81. Metz B, Davidson O, de Coninck HC, Loos M, Meyer LA, editors. IPCC Special Report on Carbon Dioxide Capture and Storage. Cambridge: Cambridge University Press; 2005.
82. Keranen KM, Weingarten M, Abers GA, Bekins BA, Ge S. Sharp increase in central Oklahoma seismicity since 2008 induced by massive wastewater injection. Science. 2014;345(6195):448–451. doi:10.1126/science.1255802.
83. Zoback MD, Gorelick SM. Earthquake triggering and large-scale geologic storage of carbon dioxide. Proc Natl Acad Sci USA. 2012;109(26):10164–10168. doi:10.1073/pnas.1202473109.
84. Holländer HM, Mayer B, Millot R, Chajewski O, Stumpp C. Isotope tracers to evaluate CO_2 fate and transport in an integrated carbon sequestration experiment. Chem Geol. 2020;548:119665. doi:10.1016/j.chemgeo.2020.119665.
85. Miri R, Hellevang H. Salt precipitation during CO_2 storage – a review. Int J Greenhouse Gas Control. 2016;51:136–147. doi:10.1016/j.ijggc.2016.05.015.
86. Fleury M, Pironon J, Le Nindre YM, Bildstein O, Berne P, Lagneau V, et al. Evaluating sealing efficiency of caprocks for CO_2 storage: an overview of the geocarbone integrity program and results. Energy Procedia. 2011;4:5227–5234. doi:10.1016/j.egypro.2011.02.502.
87. Bachu S. Screening and ranking of sedimentary basins for sequestration of CO_2 in geological media. Environ Geol. 2003;44(3):277–289. doi:10.1007/s00254-003-0762-9.
88. Espinoza DN, Kim SH, Santamarina JC. CO_2 geological storage – geotechnical implications. KSCE J Civ Eng. 2011;15(4):707–719. doi:10.1007/s12205-011-0011-9.
89. Imolore MO, Aderoju RA. Geotechnical properties and potential of a bentonite stabilized lateritic soil as landfill liners. J Earth Atmos Res. 2024;7(1):189–200.
90. Asiwaju-bello YA, Daramola SO, Owoseni JO, Olabode OF, Oladoja V, Aderoju RO, et al. Mineralogical and physical characterization of some clayey soils from parts of southwestern Nigeria for ceramic application. Int J Res Innov Appl Sci. 2025;10(11):885–897. doi:10.51584/IJRIAS.2025.101100082.
91. Taiwo BO, Melodi MM, Falade OM, Aderoju RO, Fissha Y, Akinlabi AA, et al. Evaluation of mining labor impact on production: an application of TOPSIS-CRITIC based multiple criteria decision making approach. Int J Min Geo-Eng. 2024;58(1):11–20. doi:10.22059/IJMGE.2023.358513.595061.
92. Taiwo BO, Aderoju RO, Falade OM, Fissha Y, Ogunyemi OB, Omosebi AO, Omeyoma S, Adediran OV, Bamidele HA, Ogundiran M. Mine geo-environment assessment: carbonate rock mine waste as construction material additive and coupled with pollution index model. J Min Environ. 2023;14(1):179–196. doi:10.22044/jme.2023.12691.2305

93. Falowo M, Aderoju R, Anisere O. Artificial intelligence in subsurface energy storage: a critical review of characterization, monitoring, forecasting, and risk assessment. Int J Res Eng. 2025;7(2):235–252. doi:10.33545/26648776.2025.v7.i2c.187.
94. Anisere O, Falowo M, Aderoju R. Heavy metal contamination in stream sediments: a critical review of geochemical indices, spatial distribution, and environmental risk assessment. Int J Appl Res. 2023;9(8):314–327. doi:10.22271/allresearch.2023.v9.i8d.13754.